Chinese Chemical Letters 34 (2023) 107757

Contents lists available at ScienceDirect

Chinese Chemical Letters

journal homepage: www.elsevier.com/locate/cclet

Copper-based metal-organic frameworks for electrochemical reduction of CO_2

Xiaomin Kang[a,b], Guodong Fu[a], Xian-Zhu Fu[a,*], Jing-Li Luo[a,*]

[a] Shenzhen Key Laboratory of Polymer Science and Technology, Guangdong Research Center for Interfacial Engineering of Functional Materials, College of Materials Science and Engineering, Shenzhen University, Shenzhen 518060, China
[b] School of Mechanical Engineering, University of South China, Hengyang 421001, China

ARTICLE INFO

Article history:
Received 27 May 2022
Revised 22 July 2022
Accepted 16 August 2022
Available online 21 August 2022

Keywords:
CO_2 electrochemical reduction
Cu nanoparticles
Cu-based MOFs
Electrocatalysts
Electrochemical reduction reaction

ABSTRACT

The electrochemical CO_2 reduction reaction (CO_2ER) is an emerging process that involves utilizing CO_2 to produce valuable chemicals and fuels by consuming excess electricity from renewable sources. Recently, Cu and Cu-based nanoparticles, as earth-abundant and economical metal sources, have been attracting significant interest. The chemical and physical properties of Cu-based nanoparticles are modified by different strategies, and CO_2 can be converted into multicarbon products. Among various Cu-based nanoparticles, Cu-based metal-organic frameworks (MOFs) are gaining increasing interest in the field of catalysis because of their textural, topological, and electrocatalytic properties. In this minireview, we summarized and highlighted the main achievements in the research on Cu-based MOFs and their advantages in the CO_2ER as electrocatalysts, supports, or precursors.

1. Introduction

The increasing of CO_2 emission in the earth's atmosphere is nowadays an urgent and critical issue facing humanity [1]. It further causes the rapid accumulation of greenhouse gas, melting of floating icebergs, a rise in sea level and so forth, threatening the existence and development of human race. Thus, the electrochemical conversion of electricity and CO_2 into chemicals and fuels has drawn great attention [2,3]. Electrochemical CO_2 reduction reaction (CO_2ER) is energetically and atomically inefficient caused by large kinetic overpotentials and lack in selectivity of the chemical product, especially the competition with the hydrogen evolution reaction in aqueous solutions. The CO_2 molecules get to the catalytic sites through diffusion in the aqueous phase, and several valuable products can be generated, such as carbon monoxide (CO), ethylene (C_2H_4), formic acid (HCOOH), oxalic acid ($H_2C_2O_4$) and alcohols (CH_3OH, C_2H_5OH, *etc.*) [4]. In CO_2ER, the cathodic reaction is of general form:

$$xCO_2 + nH^+ + ne^- \rightarrow \text{product}(CO, C_2H_4, HCOOH, H_2C_2O_4, \text{alcohols}, etc.) + yH_2O \quad (1)$$

while the anodic reaction in CO_2ER is oxygen evolution reaction (OER), like in water splitting in order to sum to the overall reaction [5]:

$$xCO_2 + yH_2O \rightarrow \text{product} + zO_2 \quad (2)$$

In other words, $CO_2 + 2H^+ + 2e^- \rightarrow HCOOH$, water is the only renewable and scalable source of electrons and protons [6]. Besides, the equilibrium potentials for CO_2ER have been listed in Table 1 as follows.

All the CO_2ER standard potentials are calculated *via* the Gibbs free energy of reactions using gas-phase thermochemistry and the Henry law data from National Institute of Standards and Technology (NIST) for aqueous products. Furthermore, the CO_2ER products exhibit similar reduction potentials. This explains why CO_2ER and hydrogen-evolution reaction (HER) compete since their reduction potentials are similar [7,8].

Among all the catalysts for CO_2ER, Cu and its oxides have been well developed for the electroreduction of CO_2 to high-value hydrocarbons, fuels, alcohol products, and multicarbon chemicals [9–12]. In 1989, Hori *et al.* first analyzed the gaseous and liquid products of a CO_2ER catalyzed by polycrystalline metal electrodes (Table 2) [13]. Among various metal electrodes, Cu exhibits outstanding selectivity toward hydrocarbon, aldehyde, and alcohol products. Moreover, as a pure metal, Cu can reduce CO_2 to products that require the transfer of more than two electrons with substantial Faradaic efficiencies (FEs).

* Corresponding authors.
E-mail addresses: xz.fu@szu.edu.cn (X.-Z. Fu), Jingli.Luo@ualberta.ca (J.-L. Luo).

https://doi.org/10.1016/j.cclet.2022.107757
1001-8417/

Table 1
Electrochemical reactions with equilibrium potentials.

Reaction	E_0 (V *vs.* RHE)
$CO_2 + 2H^+ + 2e^- \rightarrow CO + H_2O$	−0.52
$CO_2 + 2H^+ + 2e^- \rightarrow HCOOH$	−0.61
$CO_2 + 4H^+ + 4e^- \rightarrow HCHO + H_2O$	−0.48
$CO_2 + 6H^+ + 6e^- \rightarrow CH_3OH + H_2O$	−0.38
$CO_2 + 8H^+ + 8e^- \rightarrow CH_4 + 2H_2O$	−0.24
$2CO_2 + 12H^+ + 12e^- \rightarrow C_2H_4 + 4H_2O$	−0.34
$CO_2 + e^- \rightarrow CO_2$	−1.90
$H_2 + 2e^- \rightarrow H_2$	−0.41

Table 2
Summary of properties of various metals towards the electrochemical reduction of CO_2.

$xCO_2 + n\ H^+ + ne^-$	Catalyst	Product
	Cu	CO, hydrocarbons, aldehydes, alcohols
	Au, Ag, Zn, Pd, Ga	CO
	Pb, Hg, Tl, In, Sn, Cd, Bi	HCOOH
	Ni, Fe, Pt, Ti	H_2

Furthermore, metals are divided into four groups based on their selectivity, which depends on their binding energy to key CO_2ER and HER intermediates, including *H, *OCHO, *COOH, and *CO [14]. Specifically, Cu alone can reduce CO_2 to > $2e^-$ products [15]. This is attributed to its negative adsorption energy for *CO and positive adsorption energy for *H [16]. In addition, the multiple crystal facets, grain boundaries, and defects on the surface of metal catalysts influence their selectivity for CO_2ER products [17].

Nevertheless, various Cu(hkl) surfaces have different effects on the product distribution [18]. Thus far, according to experimental data, the surface crystal facet has been determined to have a slight effect on the catalytic activity. However, crystal defects have been shown to significantly impact the CO_2ER selectivity [19]. For instance, the Cu(111) surface shows considerably higher selectivity toward C_2 products than the Cu(751) surface, which has abundant highly undercoordinated sites [20]. Among the three Cu single-crystal facets with low indexes, *i.e.*, Cu(111), Cu(110), and Cu(100), the Cu(100) surface exhibits the highest selectivity toward C_2H_6, while Cu(111) and Cu(110) exhibit the highest selectivity toward CH_4. The Cu(100) surfaces more easily form alcohols (CH_3OH, C_2H_5OH, *etc.*) compared to formic acid at −1.00 V *vs.* reversible hydrogen electrode (RHE), while the opposite is observed for Cu(111). The Cu(110) surface exhibits high selectivity toward alcohols and carboxylates at similar rates. The C_2H_4/CH_4 ratio is plotted as a function of the crystal orientation, and the results clearly demonstrate that steps can enhance the selectivity toward C_2H_4 formation in comparison with planar single crystals [21]. Further, defects enhance the selectivity toward ethanol (C_2H_5OH) and C_2H_4.

Hori *et al.* during their tests, found that the single-crystal electrode could be reduced and reconstructed, thus leading to the formation of defects. Specifically, the reconstruction on the surface of a Cu electrode would alter the activity and product selectivity [4]. To date, the mechanisms of the CO_2ER on Cu electrodes remain unclear. However, early experiments revealed that the reduction of CO on Cu results in similar product distribution as that for reduction of CO_2 (CO_2R) on Cu, and the following research on CO reduction on Cu further supported this proposal [22]. Therefore, CO is a key intermediate in the CO_2R to hydrocarbons, aldehydes, and alcohols on Cu [23]. In detail, *CO intermediates (adsorbed CO) are bound on the Cu surface and converted into alcohols by *CO dimerization or hydrocarbons *via* *COH or *CHO intermediates [24]. Furthermore, CO adsorption on Cu can suppress the competing HER because of site-blocking effects and the changes in the *H-binding energy. This explains the high FE for CO_2R in aqueous electrolytes

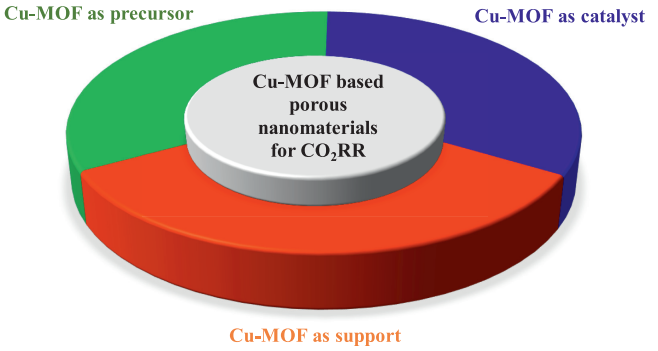

Fig. 1. Cu-MOF related catalysts engineering for CO_2ER.

[25]. Overall, Cu is a transition metal capable of catalyzing the conversion of CO_2 directly into various value-added products.

In electrocatalysis, the surface area of the catalyst significantly influences its CO_2ER activity. Cu-based catalysts have been fabricated into various shapes to enlarge their active surface areas. Among these Cu-based electrocatalysts, Cu-based metal-organic frameworks (MOFs), as porous crystalline materials consisting of a 3D framework of Cu ions or Cu clusters linked by organic linkers, have attracted significant interest for their application as electrocatalysts in CO_2ER [26–31].

Cu-based MOFs exhibit many intriguing properties, including high crystallinity and porosity, and strong metal-ligand coordination bonds; thus, they exhibit a high adsorption capacity for reaction intermediates [32–36]. Moreover, the formation of undercoordinated Cu sites in MOFs can be promoted to enhance the CO_2ER efficiency; This is attributed to the chemical tunability and the porosity/surface-topography controllability of MOFs. Thus, Cu-based MOFs can be explored as a catalytic material for better understanding the CO_2ER. However, owing to the textural properties and poor stability of MOFs, Cu-based MOFs are employed as active supports and catalyst precursors, which are either treated by pyrolysis or electrochemical reaction to afford stable and efficient electrocatalysts for the CO_2ER (Fig. 1).

2. Cu-MOF related catalysts for CO_2ER

2.1. Cu-MOF as electrocatalysts

The combination of the catalytic properties of Cu with the unique structural features of MOFs has been explored in CO_2ER research (Table 3). In particular, Cu ions coordinate with organic ligands, forming 3D network-like structures. Subsequently, the Cu centers participate in electrochemical redox processes. The coordinated Cu^{2+} can shift into transient reduced states, *i.e.*, Cu^+ and Cu^0, or transient oxidized states, *i.e.*, Cu^{3+} or Cu^{4+}.

In 2010, Angamuthu *et al.* reported a dinuclear Cu(I) complex as a reductant for CO_2ER (Fig. 2a). The Cu(II) complex could be reduced to regenerate the Cu(I) complex by treatment in acetonitrile with a soluble lithium salt at a relatively accessible potential [37].

For the application of Cu-MOF as a catalyst for CO_2ER, which was firstly investigated in 2012, Hinogami *et al.* synthesized a copper rubeanate MOF (CR-MOF) to enhance the selectivity of the CO_2ER. At the onset potential of ∼ 0.20 V, which was more positive than that for a Cu electrode in an aqueous electrolyte, formic acid was the only CO_2R product obtained on the CR-MOF electrode (*FE* ≈ 100.00%). However, the Cu electrode generated several products. Meanwhile, the quantity of products and the partial current of formic acid on the CR-MOF electrode were considerably greater than those on the Cu electrode [38].

Table 3
Summary of electrochemical reduction of CO_2 (CO_2ER) performance of Cu-MOF catalysts.

Electrocatalyst	Electrolyte	Main product	Peak FE (%)	Peak J_{total} (mA/cm^2)	Peak potential (V)	Refs.
CR-MOF	0.50 mol/L $KHCO_3$	HCOOH	~ 98.00	8.00	−1.2 (*vs.* SHE)	[38]
Cu-BTC	0.01 mol/L TBATF in DMF	Oxalic acid	Ca.51.00	19.22	−2.5 (*vs.* Ag/Ag$^+$)	[39]
Cu-BTC	0.50 mol/L $KHCO_3$	C_2H_5OH	10.30	10.00	−0.28	[41]
Cu@Zr-MOF	_	CH_3OH	–	–	–	[42]
Cu-SIM NU-1000	0.10 mol/L $NaClO_4$	HCOO-	28.0	1.20	−0.82	[43]
$Cu_3(BTC)_2$	0.50 mol/L $NaHCO_3$	CH_4	10.00	17.00	−2.5 (*vs.* SCE)	[44]
Cu^{II} phthalocyanine (Cu-MOF)	0.50 mol/L $KHCO_3$	CH_4	66.00	13.00	−1.06 (*vs.* RHE)	[46]
Cu^{II}/ade-MOFs	0.10 mol/L $KHCO_3$	CH_4	50.00	15.00	−1.60 (*vs.* RHE)	[47]
Cu_2(CuTCPP) nanosheet	0.50 mol/L EMIMBF$_4$, MeCN with 1 mol/L H_2O	$HCOO^-$	68.40	Ca. 4.50	−1.55 (*vs.* Ag/Ag$^+$)	[48]
CoPc-Cu-O	0.20 mol/L $KHCO_3$	CO	85.00	17.30	−0.63	[49]
Cu-THQ	1.00 mol/L $C_5H_{14}CINO$ & 1 mol/L KOH	CO	91.00	173.00	−0.45 (*vs.* RHE)	[50]
Cu-MOF/GO	0.10 mol/L TBAB/DMF	HCOOH	58.00	0.06	−1.00 (*vs.* SCE)	[51]
HKUST-1	0.10 mol/L $KHCO_3$	C_2H_4 & C_2H_5OH	58.60	19.20	−0.98 (*vs.* RHE)	[52]
Cu-ZIF-8	0.10 mol/L $KHCO_3$	CH_4 & CO	35.21	2.86	−1.60 (*vs.* Ag/Ag$^+$)	[53]
MOF-Cu_3(HITP)$_2$	0.10 mol/L $KHCO_3$	C_2H_4	48.00	48.00	−1.56	[54]
H-CuTCPP	0.50 mol/L EMIMBF$_4$, MeCN with 1 mol/L H_2O	Acetic acid	26.10	–	−1.60 (*vs.* Ag/Ag$^+$)	[55]

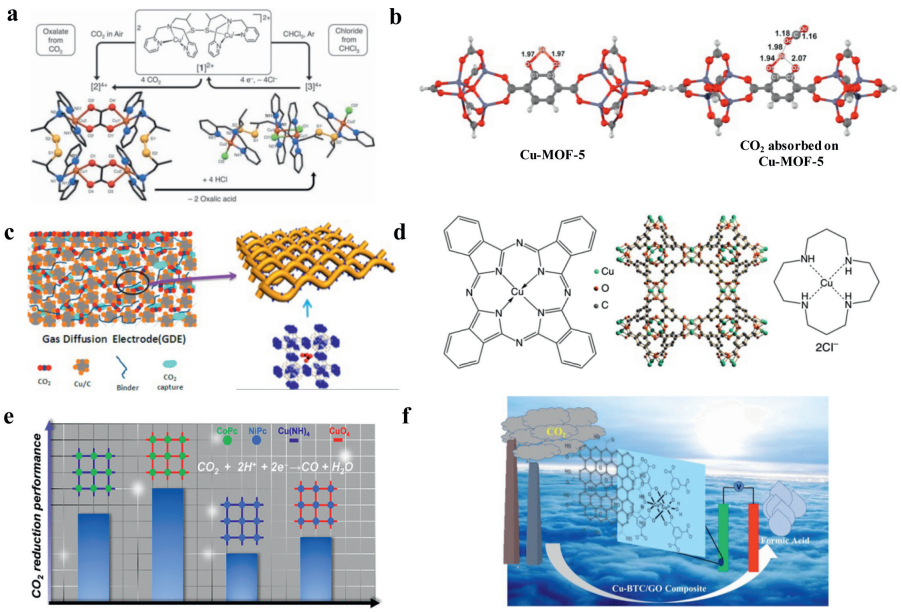

Fig. 2. Copper ions coordinated by organic ligands, resulting in 3D network structures. (a) Schematic overview of the formation and reactivity of the Cu complexes. Reproduced with permission [37]. Copyright 2010, Science. (b) Optimized structure of the models for Cu-MOF-5, and CO_2 adsorbed on Cu-MOF-5 (Ads). Reproduced with permission [40]. Copyright 2013, American Chemical Society. (c) Structural schematic diagram of GDE with $Cu_3(BTC)_2$ as CO_2 capture agent. Reproduced with permission [44]. Copyright 2018, American Chemical Society. (d) Molecular structures of three Cu-complex materials and their electrocatalytic performance for CO_2 reduction. Molecular structures of CuPc, HKUST-1, and [Cu(cyclam)]Cl_2. Reproduced with permission [46]. Copyright 2018, Springer Nature. (e) Hierarchical tuning of the performance of electrochemical carbon dioxide reduction using conductive two-dimensional metallophthalocyanine based metal-organic framework. Reproduced with permission [49]. Copyright 2020, American Chemical Society. (f) $Cu_3(BTC)_2$ metal-organic framework (Cu-MOF) and graphene oxide composite in electroreduction of CO_2 to formic acid. Reproduced with permission [51]. Copyright 2020, American Chemical Society.

Later in 2012, Kumar *et al.* prepared copper benzene-1,3,5-tricarboxylate (Cu-BTC) porous films, which exhibited excellent stability and uniform dispersion in an aqueous system as electrocatalysts loaded on glassy carbon electrodes in 0.10 mol/L KCl for CO_2ER. Cyclic voltammetric studies indicated that Cu(I) would react *in-situ* with CO_2. Moreover, by adding *N*,*N*-dimethylformamide (DMF) to saturated CO_2, oxalic acid can be obtained (FE of ~ 51.00% and a current density of 19.00 mA/cm^2). During the CO_2ER process, protons are taken from DMF through a two-electron pathway and dimerization process, thus reducing CO_2 to oxalic acid [39].

Maihom *et al.* further investigated the reaction mechanisms of CO_2 hydrogenation to formic acid over Cu-alkoxide-functionalized MOFs (Cu-MOF-5) by M06-L density functional calculations (Fig. 2b). The results revealed that the CO_2ER has two pathways: concerted and stepwise. Compared with the concerted mechanism, the stepwise mechanism firstly proceeds with hydrogen abstraction by CO_2 to yield a formate intermediate, after which another hydrogen is obtained to yield formic acid. The activation energies are approximately 24.20 and 18.30 kcal/mol for the first and second steps, respectively. These energies are considerably smaller than that for the concerted mechanism (67.20 kcal/mol). This result indicated that the stepwise mechanism was more efficient than the concerted mechanism. Moreover, the catalytic effect of Cu-MOF-5 was comparable to that achieved in a gas-phase uncatalyzed reaction with an activation energy of 73.00 kcal/mol. This further indicated that Cu-MOF-5 can be utilized as an electrocatalyst for the CO_2ER [40].

Following these pioneer works, Cu-based MOF-loaded gas-diffusion electrodes (GDE), including 1-(2-methyl-4-(2-oxopyrrolidin-1-yl)phenyl)-3-morpholino-5,6-dihydropyridin-2(1*H*)-one (HKUST-1) MOF, copper(II)–adeninate–acetate coordination framework (CuAdeAce) MOF, copper bis-bidentate dithiooxamidate (CuDTA) mesoporous metal-organic aerogel (MOA), and CuZnDTA

MOA, were employed in CO_2ER by Albo *et al*. These electrode materials exhibited excellent catalytic potentials because of their high surface areas and abundant, exposed Cu active centers, which were beneficial for CO_2ER. Furthermore, the production of methanol (CH_3OH) and C_2H_5OH in the liquid phase can be achieved with a high efficiency. The FEs for the CO_2ER on HKUST-1, CuAdeAce-, CuDTA- and CuZnDTA-based electrodes were 15.90%, 1.20%, 6.00% and 9.90%, respectively, at the current density of 10.00 mA/cm^2. Among the sample electrode materials, HKUST-1- and CuZnDTA-based electrodes exhibited outstanding and stable electrocatalytic performances [41].

In 2016, Rungtaweevoranit *et al*. utilized Zr-based MOFs to promote the activity and selectivity of a Cu catalyst. Specifically, an 18.00 nm-Cu nanocrystal was encapsulated in a UiO-66 single crystal, and it exhibited strong interaction with the Zr oxide of the MOF support. The Cu⊂UiO-66 structure induced an 8-fold enhancement in the yield and 100.00% selectivity for CH_3OH. This indicated that Cu nanocrystals embedded in MOFs can be applied to achieve high catalytic activities [42].

Kung *et al*. reported a method to anchor Cu nanoparticles (NPs) on NU-1000 thin films by installing single-site Cu(II) into the NU-1000 thin film. In the subsequent electrochemical reduction reaction, Cu(II) was reduced to metallic Cu. Furthermore, the Cu nanoparticles exhibited moderate electrocatalytic activity, with an $HCOO^-$ FE of 28.00% at −1.20 mA/cm^2 and −0.82 V *vs.* RHE [43].

Moreover, Qiu *et al*. utilized $Cu_3(BTC)_2$ (Cu-MOFs) as electrocatalysts for CO_2 capture. This material was employed in the fabrication of a GDE (Fig. 2c). The FEs of CH_4 on the GDE with Cu-MOFs were 2–3 fold higher than those on the GDE without Cu–MOFs at negative potentials (−2.30 ∼ −2.50 V *vs.* saturated calomel electrode (SCE)). Meanwhile, the FE of the competitive HER was reduced by 30%. The enhanced CO_2ER performance on the GDE with Cu-MOFs was attributed to the accumulation of CO_2 on the interface of the GDE and the electrolyte, which was attributed to the CO_2-capture properties of Cu-MOFs [44].

In 2019, An *et al*. put forward a catalyst composed of cooperative Cu(I) sites on a Zr_{12} cluster of a MOF for CO_2ER to C_2H_5OH. By introducing the alkali cation, the spatially proximate Zr_{12}-supported Cu(I) centers activate hydrogen *via* bimetallic oxidative addition and promote C-C coupling to yield C_2H_5OH. Notably, Cs^+-modified MOF catalysts yielded C_2H_5OH with > 99.00% selectivity after a 10 h reaction. This demonstrated that the catalyst can be employed as a tunable platform to design non-precious metal catalysts for future CO_2ER [45].

Apart from the above Cu-MOFs, three Cu complex materials for CO_2ER were investigated by Weng *et al*. (Fig. 2d). Among these three materials, copper(II) phthalocyanine exhibited the highest selectivity toward CH_4 with a FE of ∼ 66.00% at 13.00 mA/cm^2 and −1.06 V *vs.* RHE. *In-situ* X-ray absorption spectroscopy analysis highlighted that copper(II) phthalocyanine underwent reversible structural and oxidation state changes to form 2.00 nm-metallic Cu clusters. Density functional calculations further confirmed the molecular structure of the metal-ion ligand coordination and the dispersed Cu clusters, which contributed to the CO_2ER selectivity toward CH_4 [46].

Nevertheless, Xia *et al*. utilized Cu^{II}/adeninato/carboxylato metal-biomolecule frameworks (Cu^{II}/ade-MOFs) for CO_2ER toward hydrocarbon (CH_4, and C_2H_4) generation. The cathodized Cu^{II}/ade-MOFs exhibited excellent catalytic performance with a total hydrocarbon FE of over 73.00%. C_2H_4 was collected and measured with a maximum FE of 45.00% at 8.50 mA/cm^2 and −1.40 V *vs.* RHE, while CH_4 was obtained with a FE of 50.00% at ∼15.00 mA/cm^2 and −1.60 V *vs.* RHE. This indicated that the reconstruction of cathodized Cu^{II}/ade-MOFs and the formed Cu nanoparticles functionalized by N-containing ligands contributed to the excellent CO_2ER performance [47].

In 2019, Wu *et al*. utilized Cu(II) porphyrinic MOF nanosheets for CO_2ER and compared the results with those obtained with CuO, Cu_2O, Cu, a porphyrin-Cu(II) complex, and a CuO/complex composite. Among them, Cu-MOF nanosheets exhibited excellent formate selectivity with a FE of 68.40% at −1.55 V *vs.* Ag/Ag^+. Furthermore, the C-C coupling product, acetate, and formate were obtained in a rather wide voltage range from –1.40 V to −1.65 V with the total liquid product FE ranging from 38.00% to 85.20%. Thus, the high selectivity and catalytic activity of Cu-MOFs for CO_2R to yield formate and acetate should be attributed to the synergistic enhancement of the porphyrin-Cu(II) complex [48].

In addition to the above structures, four systematic structural analogs of conductive 2D MOFs composed of metallophthalocyanine (MPc) ligands linked by Cu nodes for CO_2ER to CO were investigated by Meng *et al*. (Fig. 2e). The catalytic activity and selectivity of the MOFs were determined hierarchically by two structural factors: the metal within the MPc (M = Co *vs.* Ni) catalytic subunit and the identity of the heteroatomic cross-linker (X) between the subunits (X = O *vs.* NH). Furthermore, these properties were governed by the metal within the MPcs and further modulated by the heteroatomic linkages. Among these MOFs, CoPc-Cu-O exhibited the highest selectivity toward CO (as a composite with carbon black in 1:1 mass ratio; FE_{CO} = 85.00% at the current density of −17.30 mA/cm^2) at −0.63 V. Without any conductive additives, CoPc-Cu-O, when employed directly as an electrode material, exhibited excellent performance at a current density of −9.50 mA/cm^2 with a FE_{CO} of 79.00% [49].

In 2021, copper tetrahydroxyquinone (Cu-THQ), which is a 2D Cu-based conductive MOF with an average lateral size of 140 nm, was fabricated by Salehi-Khojin *et al*. for aqueous CO_2ER at low overpotentials. It exhibited a high current density of ∼173.00 mA/cm^2 at −0.45 V *vs.* RHE, an average FE of ∼ 91.00% toward CO production, and an excellent turnover frequency of ∼20.82 s^{-1}. When Cu-THQ was employed for CO_2ER to yield CO, it exhibited 35 and 25 times higher activities than those of state-of-the-art MOFs and MOF-derived catalysts, respectively. The experimental and DFT results both revealed the existence of reduced Cu (Cu^+) during the CO_2ER, which reversibly converts into Cu^{2+} after the reaction [50].

Jeong *et al*. designed a Cu-based MOF (Cu-benzene-1,3,5-tricarboxylic acid) along with graphene oxide (GO) for CO_2ER. The Cu-MOF/GO electrocatalyst was employed in different supporting electrolytes, including $KHCO_3/H_2O$, tetrabutylammonium bromide (TBAB)/DMF, KBr/CH_3OH, CH_3COOK/CH_3OH, TBAB/CH_3OH, and tetrabutylammonium perchlorate (TBAP)/ CH_3OH (Fig. 2f). After conducting CO_2ER at various polarization potentials, the results showed that HCOOH was the main product. The highest concentrations of HCOOH formed were 0.14 mmol/L (at −0.10 V), 66.57 mmol/L (at −0.60 V), 0.27 mmol/L (at −0.50 V), 0.24 mmol/L (at −0.50 V), 0.78 mmol/L (at −0.40 V), and 0.31 mmol/L (at −0.45 V) in $KHCO_3/H_2O$, TBAB/DMF, KBr/CH_3OH, CH_3COOK/CH_3OH, TBAB/CH_3OH, and TBAP/CH_3OH supporting electrolyte systems, respectively. A high FE of 58.00% was obtained in 0.10 mol/L TBAB/DMF, whereas with Cu-MOF alone, the efficiency was 38.00%. Jeong *et al*. demonstrated that the synergistic effect of GO sheets at a concentration of 3.00 wt% and the Cu^+-OH^- interaction both contributed to the formation of formic acid in various electrolytes [51].

Recently, the facile electrodeposition of an HKUST-1 thin film on carbon paper was investigated by Wang *et al*. Their findings indicated that the CO_2ER activity was highly affected by the structural reconstruction of HKUST-1. The HKUST-1 film was reconstructed into two structures during the CO_2ER process. Three-dimensional nanospheres (numerous small fragments) and 3D nanonetworks (cross-linked nanobelts in different directions) were formed during the CO_2ER over time. The 3D nanosphere

Table 4
Cu-MOF as electrocatalyst precursors.

Electrocatalyst	Electrolyte	Main product	Peak FE (%)	Peak J_{total} (mA/cm^2)	Peak potential (V)	Refs.
OD-Cu/C	0.10 mol/L $KHCO_3$	CH_3OH	~ 43.20	~ 8.90	−0.30	[56]
MOF derived Cu clusters	1.00 mol/L KOH	C_2H_4	45.00	262.00	−1.07	[57]
M(Ni, Cu, Fe and Co)-N_4@MOF	0.50 mol/L $KHCO_3$	CO	30.00	0.10	−0.70 (*vs.* RHE)	[58]
Cu-MOF	0.50 mol/L $KHCO_3$	CO	43.80	230.00	−0.86	[59]
MOF-derived In-Cu bimetallic oxides	0.50 mol/L $KHCO_3$	CO	92.10	11.20	−0.80	[60]
Cu MOF-NC	0.10 mol/L $KHCO_3$	C_2H_5OH	18.40	8.00	−1.01 (*vs.* RHE)	[61]
PcCu-O_8-Zn	0.10 mol/L $KHCO_3$	CO	88.00	2.80	−0.70 (*vs.* RHE)	[62]
Cu@Cu_xO MOF	0.10 mol/L $KHCO_3$	C_2H_4	51.00	150.00	−1.58 (*vs.* RHE)	[63]
Cu-N_2 derived from Cu-BTC	0.10 mol/L $KHCO_3$	CH_4	38.60	14.80	−1.60	[64]
Cu-BTT derived Cu-NC	0.10 mol/L $KHCO_3$	CO/HCOOH	40.80/38.10	0.40/1.40	−0.60/−0.90 (*vs.* RHE)	[65]
Fe_xCu-MOF	0.10 mol/L $KHCO_3$	CO	48.50	21.00	−1.30 (*vs.* Ag/Ag$^+$)	[66]
Cu–GNC–VL	0.50 mol/L $KHCO_3$	C_2H_5OH	70.53	10.40	−0.87 (*vs.* RHE)	[67]
HKUST-MOF derived $Cu_xO_yC_z$	1.00 mol/L KOH	C_{2+} (C_2H_4, C_2H_6, C_2H_5OH, 1-C_3H_7OH)	54.00	80.00	–	[68]
Cu-In/C	0.10 mol/L $KHCO_3$	CO	85.00	4.00	−0.75 (*vs.* RHE)	[69]
CuZn-NC	0.10 mol/L $KHCO_3$	C_2H_4, C_2H_5OH	25.00	12.00	−1.00 (*vs.* RHE)	[70]
Cu_2O/Cu@NC	0.10 mol/L $KHCO_3$	CH_4/C_2H_4	20.40/23.90	–	−1.40/1.60 (*vs.* RHE)	[71]
MOF derived Cu catalyst	0.10 mol/L $KHCO_3$	CH_4	50.00	3.50	−1.30 (*vs.* RHE)	[72]
Cu@Cu_2O NC	0.50 mol/L $KHCO_3$	CH_3OH	45.00	–	−0.70 (*vs.* RHE)	[73]
MOF derived Cu/Bi catalyst	0.50 mol/L $KHCO_3$	HCOOH	93.00	10.10	−0.94 (*vs.* RHE)	[74]
Ag/Cu catalyst derived from Cu-MOF	1.00 mol/L KOH	$C_2 = C_2H_4$, C_2H_6, C_2H_5OH, C_3H_7OH/HCOOH	21.00/40.00	120.00/60.00	−0.28/−0.44 (*vs.* RHE)	[75]
Cu dendrites derived from Cu-MOF	0.50 mol/L BminBF_4, MeCN with1 mol/L H_2O	HCOOH	98.20	102.10	−1.85 (*vs.* Ag/Ag$^+$)	[75]
Cu/Cu_2O@NG	0.20 mol/L KI	C_2-C_3 products (C_2H_4, C_2H_5OH, and n-propanol).	56.00	19.00	−1.90 (*vs.* RHE)	[76]
Cu clusters from MOF	1.00 mol/L KOH	CH_4	51.20	> 150.00	–	[77]
Cu-nanosheet (MOF) structured catalyst	0.10 mol/L $KHCO_3$	HCOOH & C_2	56.00	–	−1.03 (*vs.* RHE)	[78]

structure exhibited enhanced catalytic activity, attributed to its abundant active sites, relatively low charge-transfer resistance, and high Cu^+/Cu^0 ratio. The FEs of C2 product (C_2H_4 and C_2H_5OH) were 58.60% at −0.98 V *vs.* RHE [52].

Studies have shown that the doping amount of Cu plays a key role in the catalyst structure and catalytic activity for CO_2ER. Thus, a series of Cu-doped ZIF-8 catalysts with different Cu^{2+} doping amounts, obtained by solvothermal synthesis method, was investigated by Iqbal *et al*. Among the various Cu-ZIF-8 catalysts, Cu30%ZIF-8 exhibited the highest current density of −40.00 mA/cm^2 at −2.10 V *vs.* Ag/AgCl and selectivity toward CH_4 and CO compared to previously obtained results on Cu electrodes. The excellent CO_2R performance of the as-prepared catalyst was attributed to its crystalline nanostructure with abundant Cu active metal sites and N, micro–*meso* dual porosity, and the broad surface area of the ZIF structure [53].

Recently, Peng *et al*. investigated semiconductive MOF-Cu_3(HITP)$_2$ (HITP = 2,3,6,7,10,11-hexaiminotriphenylene) as a catalyst for the CO_2ER. In comparison with the MOF alone, the combination with Ketjen Black would promote the selectivity toward C_2H_4 with FEs of 60.00%-70.00% in a wide potential range. Multicrystalline Cu nanocrystallites were induced in the reconstructed MOF and stabilized by the conducting support *via* current shock and charge delocalization. The action mechanism of this catalyst is similar to that of dendrite prevention through conductive scaffolds in metal-ion batteries. DFT calculations revealed that the multifacets and rich grain boundaries both promoted C-C coupling while suppressing the HER [54].

Above all, Xiao *et al*. investigated an electrocatalyst derived from a helical Cu-porphyrinic MOF meso–tetra (4-carboxyphenyl) porphyrin (TCPP) on Cu(OH)$_2$ nanoarrays (H-CuTCPP). The catalysts exhibited an extraordinary excellent acetic acid production whose FE was of 26.10% at −1.60 V *vs.* Ag/Ag$^+$, which was much higher than that of non-helical CuTCPP whose FE was of 19.80%. The high efficiency was attributed to the efficient utilization of the space derived from helical MOF nanoarrays. It contributed to the large amount of the active catalytic sites. Besides, the results also indicated that H-CuTCPP exhibited stronger CO linear adsorption which was in favor of producing acetic acid [55].

2.2. Cu-MOF as electrocatalyst precursors

Attributed to their poor stability, particularly at high negative potentials, Cu-MOF, as precursors, undergo further treatment (pyrolysis or electrochemical reaction) to fabricate more stable and efficient electrocatalysts (Table 4).

2.2.1. Cu-MOF treated by pyrolysis

Cu-MOF can be pyrolyzed to fabricate more stable and active electrocatalysts. In 2017, Zhao *et al*. utilized a Cu-based MOF (HKUST-1) as a precursor, and after a facile carbonization process, oxide-derived Cu/carbon (OD Cu/C) catalysts were obtained (Fig. 3a). The catalysts exhibited high selectivity toward alcohols in the CO_2ER with a total FE of 45.20%-71.20% at −0.10 ~ −0.70 V *vs.* RHE. This indicated that the onset potential for C_2H_5OH formation was approximately −0.10 V *vs.* RHE, which is among the lowest overpotentials reported. Thus, the enhanced activity and selectivity of the oxide-derived Cu/carbon might be attributed to the synergistic effect between the highly dispersed Cu and the porous carbon matrix [56].

Later, Nam *et al*. designed a strategy that involved the formation of MOF-regulated Cu clusters, which shifted the CO_2ER selectivity toward multiple-carbon-atom-containing products. The symmetrical Cu dimer was distorted into an asymmetric motif by the separation of adjacent benzene tricarboxylate moieties under thermal treatment (Fig. 3b). Cu clusters with low coordination numbers were formed from distorted Cu dimers in HKUST-1 during the CO_2ER, thus resulting in a FE of 45.00% for C_2H_4 [57].

In addition to Cu-MOF, which are applied alone as precursors, porous porphyrinic triazine frameworks with atomically isolated M-N_4 (M = Ni, Cu, Fe and Co) sites were fabricated *via* pyrolysis for the CO_2ER to CO. Among them, Ni single atoms/porphyrinic triazine framework (NiSAs/PTF) exhibited the highest FE of 98.00% at a mild potential of −0.80 V *vs.* RHE. Moreover, the mechanisms of

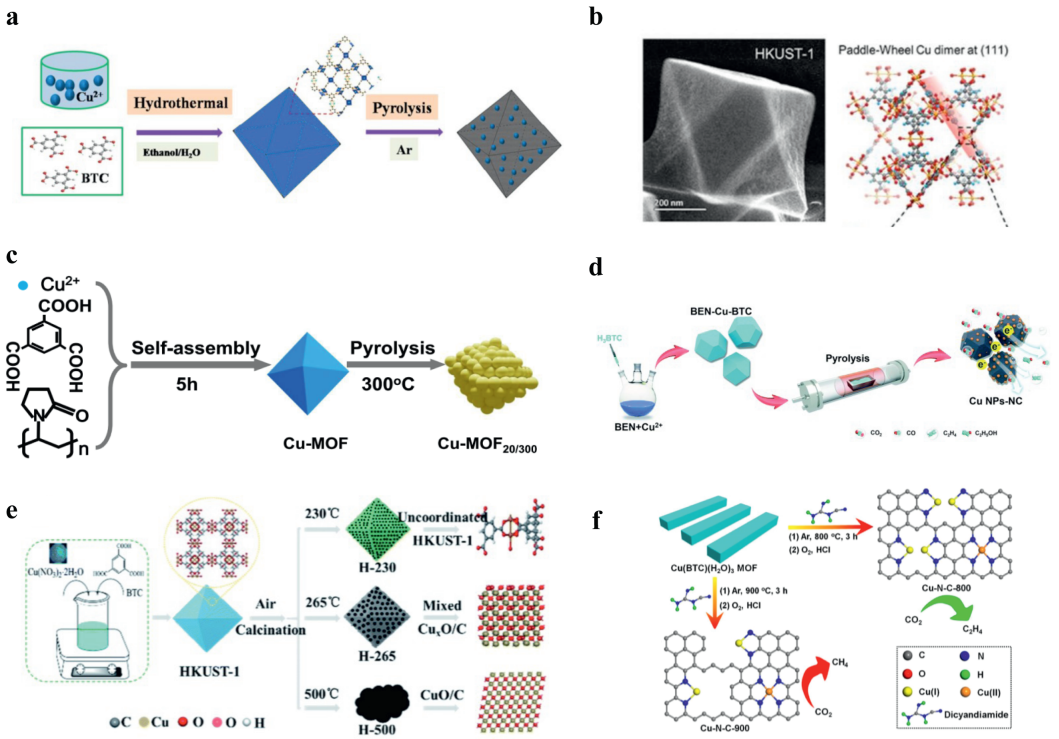

Fig. 3. Cu-MOF as precursor under pyrolysis treatment in CO_2ER. (a) The synthesis process of oxide-derived Cu/carbon catalysts. Reproduced with permission [56]. Copyright 2017, American Chemical Society. (b) Comparison of paddle-wheel structured HKUST-1 *vs.* CuAc. Structural investigations of as-fabricated HKUST-1 by SEM. Reproduced with permission [57]. Copyright 2018, American Chemical Society. (c) Illustration of the synthesis procedure of the Cu-MOF/NP catalysts. Reproduced with permission [59]. Copyright 2019, American Chemical Society. (d) Schematic illustration fabrication process for the Cu-NC composite. Reproduced with permission [61]. Copyright 2019, Royal Society of Chemistry. (e) Schematic illustration of the catalyst synthesis process (red oxygen atoms relate to CuO, pink oxygen atoms relate to Cu_2O). Structural investigations of H-265. Reproduced with permission [63]. Copyright 2020, Royal Society of Chemistry. (f) Schematic of the procedure to synthesize the Cu-N-C-T catalysts. $Cu(BTC)(H_2O)_3$ MOF precursor. Cu-N-C-800 synthesized by pyrolysis of $Cu(BTC)(H_2O)_3$ MOF and dicyandiamide at 800 °C, which favors the CO_2ER toward C_2H_4. Cu-N-C-900 derived from the pyrolysis of $Cu(BTC)(H_2O)_3$ MOF and dicyandiamide at 900 °C, which favors the CO_2ER toward CH_4. Reproduced with permission [64]. Copyright 2020, American Chemical Society.

the catalytic CO_2-CO conversion reaction over the different active M-N_4 sites were unraveled by the combination of DFT calculations and experiments [58].

Inspired by previous studies, Liu *et al.* designed a Cu-MOF-derived nanoparticle as a catalyst for CO_2ER (Fig. 3c), in which Cu/Cu_2O particles formed a porous octahedral structure containing tunable Cu and Cu^I catalytic active sites. The CO_2ER could be realized with a high current density of 25.15 mA/cm^2 at −0.79 V *vs.* RHE, which is attributed to the high surface area derived from the porous structures with exposed metal ions. Moreover, a new flow electrochemical reactor integrated with a membrane electrode assembly was designed to reduce the applied potential by approximately 200.00 mV and promote the sensitivity of the reactor for identifying and quantifying products [59].

Guo *et al.* introduced a method for tuning the selectivity of the CO_2ER to yield CO, using a MOF-derived bimetallic oxide catalyst. MOF-derived In-Cu bimetallic oxides were synthesized through the pyrolysis of an In-Cu bimetallic MOF. By altering the In/Cu ratio, the FE of CO could reach up to 92.10% at a current density of ~ 11.20 mA/cm^2. Guo *et al.* believed that the outstanding performance of the catalyst was attributed to the strong CO_2 adsorption, high electrochemical surface area, and low charge-transfer resistance of the bimetallic catalyst [60].

Furthermore, Wei *et al.* developed a MOF-derived Cu@NC catalyst by the calcination of N-containing benzimidazole-modified Cu-BTC MOFs (BEN-Cu-BTC) at various temperatures (Fig. 3d). The Cu-NC samples exhibited N-species- and content-dependent catalytic activities for the highly selective electroreduction of CO_2 to C_2 products. The results indicated that the high content of the pyrrolic-N and Cu-N species formed by the pyrolysis process at 400 °C can facilitate the production of C_2 on the Cu surface, with reaction rates and FEs for C_2H_4 and C_2H_5OH of $r_{CH_2H_4} = 5.38$ μmol m^{-2} s^{-1} (FE = 11.20%) and $r_{C_2H_5OH} = 8.83$ μmol m^{-2} s^{-1} (FE = 18.40%) at −1.01 V (*vs.* RHE), respectively. This further demonstrated that the catalytic activity can be controlled by N-type species, which are affected by the corresponding annealing temperature. Furthermore, the Cu-NC catalysts exhibited excellent electrochemical stability for over 8 h [61].

Inspired by previous studies, a layer-stacked, bimetallic 2D conjugated MOF (2D c-MOF) was designed with copper phthalocyanine as the ligand (CuN_4) and zinc-bis(dihydroxy) complex (ZnO_4) as the linker (PcCu-O_8-Zn). The PcCu-O_8-Zn complex exhibited a high CO selectivity of 88.00%. The catalytic process followed a synergistic mechanism, in which ZnO_4 complexes acted as CO_2ER catalytic sites, while CuN_4 centers promoted the protonation of adsorbed CO_2 during the CO_2ER [62].

Furthermore, a catalyst derived from Cu-MOFs (Fig. 3e) for CO_2 conversion into C_2H_4 conversion was proposed by Yao *et al.*, which exhibited enhanced performance because of its porous morphology, complex oxidation states, and strong lattice strain. The Cu@Cu_xO core-shell structure promoted the activation of CO_2, attributed to the formation of Cu^+/Cu^0 interfaces *via* stabilized $Cu^+$to facilitate *CO-CO dimerization. This accelerated the conversion of CO_2 into C_2 products but suppressed the conversion to C_1 products. The catalyst exhibited a 51.00% FE for C_2H_4 with a current density of 150.00 mA/cm^2 in a flow cell and a 70.00% FE for C_2 products in an H-cell with excellent stability [63].

Inspired by the significant research interest received by single-atom catalysis, a single-atom Cu catalyst dispersed on N-doped carbon by a N-coordination strategy was proposed by Guan *et al*. They highlighted that Cu-N_x configurations have a high catalytic activity for CO_2ER. Furthermore, the Cu-doping concentration and Cu-N_x configurations were adjusted as a function of the pyrolysis temperature (Fig. 3f). When the Cu concentration reached 4.90%, the distance between neighboring Cu-N_x species decreased, further promoting the C-C coupling and the production of C_2H_4. However, the concentration of Cu was lower than 2.40%, and the distance between the Cu and N_x species was large, which led to the formation of CH_4. DFT results further verified that two CO intermediates binding on two adjacent Cu-N_2 sites promoted the production of C_2H_4, while the isolated Cu-N_4, neighboring Cu-N_4, and isolated Cu-N_2 sites facilitated the formation of CH_4 [64].

Moreover, Cao *et al*. fabricated a N-doped Cu-NC composite electrocatalyst using a N-rich Cu-BTT MOF precursor (H_3BTT = 1,3,5-benzenetris tetrazolate) by pyrolysis. Among the various pyrolysis temperatures applied, 1100 °C was the optimal temperature at which Cu-NC (Cu-NC@1100 °C) exhibited the best catalytic activity for CO (−0.60 V *vs.* RHE, $j_{CO} = 0.40\ mA/cm^2$) and HCOOH production (−0.90 V *vs.* RHE, $j_{HCOOH} = 1.40\ mA/cm^2$). This abnormal activity might be due to the synergistic effect of the low-density-dispersed Cu nanoparticles (∼ 27 nm), large porous volume, rich pyrrolic-N and Cu-N_x active sites, and stable CO_2 adsorption [65].

Furthermore, Teng *et al*. prepared an Fe-Cu-BTT composite by introducing the Fe ion into a microporous N-rich MOF, and they employed it as a precursor. After the pyrolysis process, the Fe_XCu-NC catalyst exhibited an excellent selectivity toward CO. The FE of the catalyst pyrolyzed at 800 °C reached 48.50%, which was attributed to the Brunauer-Emmett-Teller surface area, total pore volume, Fe-N_x sites, and the low density of the Cu nanoparticles in the carbon matrix [66].

Moreover, a Cu/Cu_2O nanocomposite loaded on the surface of carbon derived from ZIF-L coated vertically on GO (Cu-GNC-VL) by pyrolysis was proposed by Zhang *et al*. The catalyst exhibited an excellent FE of 70.52% for C_2H_5OH production at a current density of $10.40\ mA/cm^2$ and −0.87 V *vs.* RHE, which benefited from the synergy between the CO_2 asymmetric chemical adsorption on Cu(111) and the suitable kinetics and thermodynamics of the C–C coupling on Cu_2O(111) [67].

Recently, Schuhmann *et al*. developed a series of $Cu_xO_yC_z$ electrocatalysts obtained from a Cu-based MOF as a porous self-sacrificial template. By modifying the GDEs with Polytetrafluoroetylene (PTFE), 25.00–50.00 wt% teflonized GDEs were obtained, which exhibited a FE of 54.00% at $-80.00\ mA/cm^2$ for C_2 products. The local OH^- activity of the PTFE-modified GDEs was evaluated using a closely positioned Pt nanoelectrode. The OH^-/H_2O activity ratio increased with the current density because of the locally generated OH^- ions, irrespective of the PTFE amount [68].

As mentioned above, single-atom catalysis of CO_2ER has been widely investigated. Lu *et al*. fabricated atomically dispersed Cu species on N-doped carbon nanosheet composite materials (Cu-NC) obtained by MOF derivatization. The Cu-NC materials exhibited better catalytic performance for the synthesis of methyl *N*-phenylcarbamate in 71.00% yield, compared with the results obtained with traditional Cu bulk electrodes at ambient temperature and normal pressure. The as-prepared catalyst exhibited excellent stability, and its catalytic activity did not decrease even after 10 consecutive cycles. Furthermore, with the Cu-NC material, a variety of amines could be turned into corresponding carbamates smoothly after the reaction [69].

By incorporating alloys into the structure of Cu-MOFs, it is possible to enhance their catalytic properties. Thus, Zhang *et al*. fabricated a Cu-In/C bimetallic catalyst by the pyrolysis of Cu-In MOF materials. The Cu-In/C catalyst with a molar ratio of 9:1 exhibited a high CO selectivity of up to 85.00% at −0.75 V *vs.* RHE, compared with the 3.10% and 10.80% achieved on Cu/C and In/C, respectively. The excellent performance was attributed to the formation of Cu_4In derived from In distributed on the surface of Cu nanoparticles, which changed the geometric and electronic structures of the Cu surface. These modifications affected the adsorption properties of the catalyst for *H, CO_2, and the intermediates during the CO_2ER; thus, the electrochemical conversion of CO_2 to CO was accelerated, and hydrogen evolution was suppressed. The large electrochemically active surface area and accelerated charge-transfer and reaction kinetics of this Cu-In bimetallic catalyst also promoted the CO_2ER activity [70].

Apart from the Cu-In/C bimetallic catalyst, a CuZn bimetallic material embedded on carbon electrocatalysts through a one-step MOF carbonization was fabricated and investigated by Rungtaweevoranit *et al*. The CuZn alloy exhibited the highest improvement (5-fold) in FE for the C_2 products (C_2H_4 and C_2H_5OH) at −1.00 V *vs.* RHE, compared with that for its Cu counterpart, far outperforming the catalyst with segregated Cu and Zn phases. This excellent performance was attributed to the influence of Zn on the electronic structure of the Cu sites [71].

Peng *et al*. designed a Cu_2O/Cu@NC catalyst derived from a Cu-NBDC MOF (a Cu-based MOF synthesized using 2-aminoterephthalic acid (NBDC) as the ligand) by annealing at different temperatures. The results indicated that Cu_2O/Cu@NC exhibited better CO_2R activity and multielectron product selectivity than Cu_2O/Cu@C. The FE increased with increasing temperature, while those of C_2H_4 and CH_4 decreased with increasing temperature. Upon pyrolysis at 400 °C, the FE of Cu_2O/Cu@NC-400 was over 86.00% at −1.40 and −1.60 V *vs.* RHE, including a FE_{C2H4} of 20.40% at −1.40 V *vs.* RHE and FE_{CH4} of 23.90% at −1.60 V *vs.* RHE. However, the FE for CH_4 (−1.60 V *vs.* RHE) of Cu_2O/Cu@C-400 without N doping was only approximately 2.33%, and no C_2H_4 was detected. These differences in the catalytic behavior were derived from the fact that Cu-N was conducive for the stable adsorption of the $*CH_2$ intermediate during the CO_2ER, thus inhibiting the evolution of H_2 [72].

Yang *et al*. proposed a novel Cu@Cu_2O NC electrocatalyst which exhibited excellent performance in converting CO_2 into methanol derived from Cu-BTC after pyrolysis at 400 °C. The optimized catalyst exhibited excellent FE of 45.00% at −0.70 V *vs.* RHE. It was attributed to the synergistic effect between Cu^0 and Cu^+ ions on the surface which contributed to the adsorption of CO_2 and the following formation of methanol [73].

A Cu/Bi bimetal catalyst was obtained by calcination of the MOF precursor under inert atmosphere. The Bimetal structure contributed to the stronger adsorption for CO_2 intermediate in comparison with Bi/Bi_2O_3@C without Cu species. The Cu/Bi catalyst exhibited extraordinary selectivity towards HCOOH with FE of about 93.00% at −0.94 V *vs.* RHE [74].

Sikdar *et al*. developed an Ag/Cu bimetallic catalyst *via* a redox replacement process on the Cu/C catalyst which was fabricated by pyrolysis of Cu-MOF. The catalyst exhibited good performance in producing C2 product (C_2H_4, C_2H_6, C_2H_5OH, C_3H_7OH) with FE of 21.00% and HCOOH with FE of 40.00%. The results in the work indicated that the formation of adsorbed *CO followed by consumption of CO in the successive cascade steps contributed to yielding HCOOH and C-C coupled products [75].

2.2.2. Cu-MOF treated by an electrochemical reaction

Apart from applying the Cu-MOF as a precursor to yield the Cu-NC catalyst *via* further pyrolysis, Cu-MOFs can also be converted into Cu-nanoparticle-embedded carbon catalysts *via* an electrochemical reaction. Kim *et al*. proposed a method using Cu-based MOF-74 as the precursor to produce Cu nanoparticles *via*

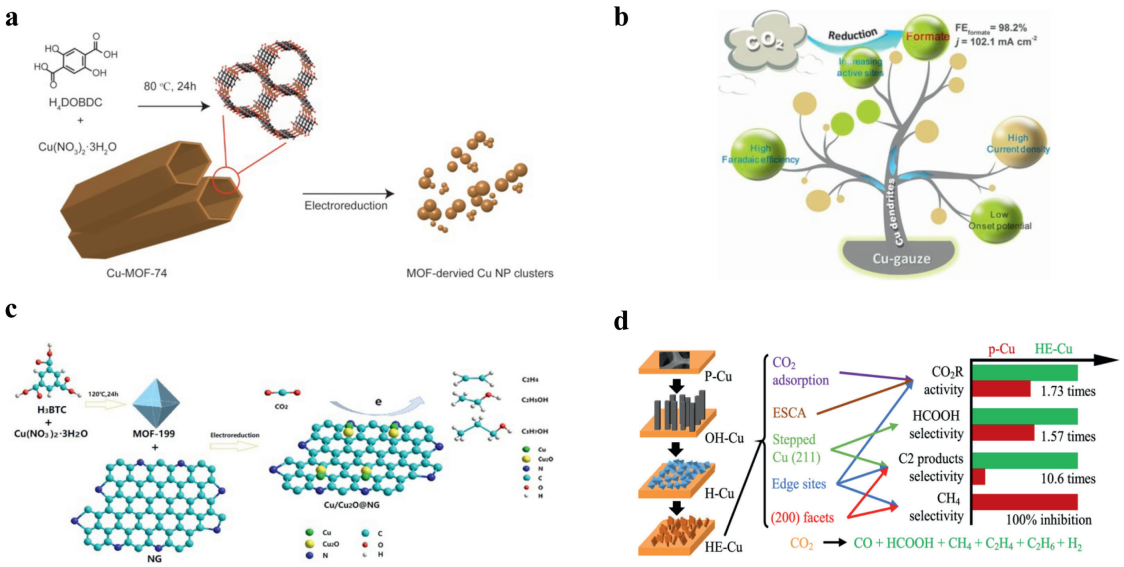

Fig. 4. Cu-MOF as precursor undergoes electrochemical treatment in CO_2ER. (a) Schematic illustration of the hydrothermal synthesis of Cu-MOF-74 and preparation of Cu NPs from Cu-MOF-74 by electroreduction. Reproduced with permission [76]. Copyright 2019, Elsevier. (b) Electrodeposited hollow metal organic framework mediated *in-situ* synthesis of copper dendrites with abundant active sites show outstanding performance for electroreduction of CO_2 to formate. Reproduced with permission [77]. Copyright 2020, John Wiley and Sons. (c) The preparation and schematic CO_2R of Cu/Cu_2O@NG from MOF-199 and NG. Reproduced with permission [78]. Copyright 2021, Elsevier. (d) Schematic diagram of electrochemical CO_2R of HE-Cu and p-Cu. (Catholyte: 0.10 mol/L CO_2 bubbled $KHCO_3$, anolyte: 0.50 mol/L NaOH and 25 °C, CO_2R activity and HCOOH selectivity potential: −1.03 V, C_2 products selectivity and CH_4 selectivity potential: −1.19 V). Reproduced with permission [80]. Copyright 2021, Elsevier.

an electrochemical reduction process (Fig. 4a). The MOF, due to its porous structure, acted as a template for the fabrication of isolated Cu-nanoparticle clusters with high catalytic activities and high efficiencies for the CO_2ER to CH_4. The MOF-derived Cu nanoparticles demonstrated high FEs of > 50.00% for CH_4 at −1.30 V *vs.* RHE [76].

Moreover, Han *et al.* reported a strategy for fabricating heterogeneous electrocatalysts composed of 3D hierarchical Cu dendrites (Fig. 4b). Traditional electrode materials (*i.e.*, Sn and In) often suffer from a low activity for CO_2 conversion into formate. Moreover, the CO_2ER yields a single product at high current densities and efficiencies. By an *in-situ* electrosynthesis method, a hollow-structured Cu-MOF film could be obtained in only 5 min. This indicated that more active sites could be exposed using this synthesis strategy, which is beneficial for the reduction of CO_2 to formate. Notably, the current density could reach 102.10 mA/cm^2 with a selectivity of 98.20% in an ionic-liquid-based electrolyte [77].

Apart from the *in-situ* electrosynthesis method, Zin *et al.* reported a simple MOF-derivatization strategy to fabricate electrocatalysts (Fig. 4c). Using MOF-199 and N-doped graphene (NG) as precursors, they carried out electroreduction to obtain Cu/Cu_2O@N-doped graphene (Cu/Cu_2O@NG) materials for efficient CO_2ER to produce C_2-C_3 products (C_2H_4, C_2H_5OH and *n*-propanol). A series of Cu/Cu_2O@NG materials, particularly Cu/Cu_2O@NG-2 with a FE of 56.00% and a current density of 19.00 mA/cm^2, were produced to afford C_2-C_3 products. The excellent performance was ascribed mostly to the synergistic effect between Cu/Cu_2O and NG, which resulted in good CO_2 adsorption, rapid mass transfer, and abundant active sites [78].

Moreover, an electrochemical oxidation–reduction method to prepare Cu clusters from MOFs was put forward by Zeng *et al.* The as-prepared Cu clusters exhibited a FE of 51.20% for CH_4 at a current density of > 150.00 mA/cm^2. These results suggested that the distinctive CH_4 selectivity is attributed to the sub-nanometer size of the derived materials; moreover, the stabilization of the clusters by the residual ligands of the pristine MOF also contributed to the distinctive selectivity [79].

A Cu-nanosheet-structured catalyst derived from the HKUST-1 MOF by an *in-situ* electrochemical reaction was proposed by Song *et al.* (Fig. 4d). The as-prepared electrochemical derivation from HKUST-1catalyst (HE-Cu) exhibited a superior FE of 56.00% compared with that of the pristine Cu foil (p-Cu, FE of 32.30%) at −1.03 V *vs.* RHE. HE-Cu exhibited a relatively low CO_2R onset potential, a higher CO_2 adsorption capacity (1.58-fold), and a larger electrochemical active surface area (1.24-fold) compared to those of p-Cu. The FEs of HCOOH and the C_2 products for HE-Cu increased by 1.57-fold and 10.6-fold at −1.19 V *vs.* RHE, respectively, compared with those of p-Cu. The excellent CO_2R activity and HCOOH and C_2 product selectivity for HE-Cu were attributed to its stepped Cu(211) surfaces, (200) facets, and Cu edge atoms [80].

2.2.3. Cu-MOFs as active supports

Apart from direct application as electrocatalysts, Cu-MOFs can also be used as active supports for CO_2ER, attributed to the textural properties and active sites of MOFs (Table 5). In 2019, Tan *et al.* prepared a catalyst by the *in-situ* etching of a Cu_2O sphere with H_3BTC to obtain a Cu-MOF shell as a support to further synthesize a Cu_2O@Cu-MOF electrocatalyst (Fig. 5a). The catalyst exhibited outstanding performances for the formation of hydrocarbons from CO_2, with a FE of 79.40% for CH_4 and C_2H_4. Moreover, the FE for CH_4 was determined to be up to 63.20% at −1.71 V [81]. As shown in Fig. 5b, Cu-MOFs used as supports contribute to the productivity of and selectivity toward CH_4 and other valuable products.

In 2021, Sun *et al.* proposed a molecular encapsulation strategy to enrich intermediates to facilitate the electrochemical conversion of CO_2 to C_2H_4. They employed metal (FeCl, Co and Ni) tetrakis(4-carboxyphenyl) porphyrin (M-TCPP) with a Cu-MOF to create a series of metalloporphyrin-decorated Cu catalysts with a coral-like shape (Fig. 5c). As shown in Fig. 5d, the possible reaction route suggests that the M-TCPP in the catalysts provides more CO intermediates to the Cu sites, enhancing the selectivity toward C_2H_4 with a FE of 33.42% at −1.17 V *vs.* RHE on the Fe-TCPP@Cu electrode compared to that on the Cu electrode (16.85%, at −1.27 V *vs.* RHE). In addition, the metalloporphyrin-decorated Cu catalysts exhibited better performance than the physical mixture of Cu-MOFs

Table 5
Cu-MOF as active support.

Electrocatalyst	Electrolyte	Main product	Peak FE (%)	Peak J_{total} (mA/cm^2)	Peak potential (V)	Refs.
Cu_2O@Cu-MOF	0.10 mol/L $KHCO_3$	CH_4	63.20	−14.00	−1.71	[81]
M-TCPP@Cu-MOF	0.50 mol/L $KHCO_3$	C_2H_4	33.42	−12.00	−1.17	[82]
CuO@Cu-MOF	0.10 mol/L $KHCO_3$	C_2H_4	50.00	–	−1.10 (*vs.* RHE)	[83]
HKUST-1–5C-Zn	0.10 mol/L $TBAPF_6$ in DMF/H_2O (9/1) solution	CO	80.00	5.60	−1.80 (*vs.* SHE)	[84]

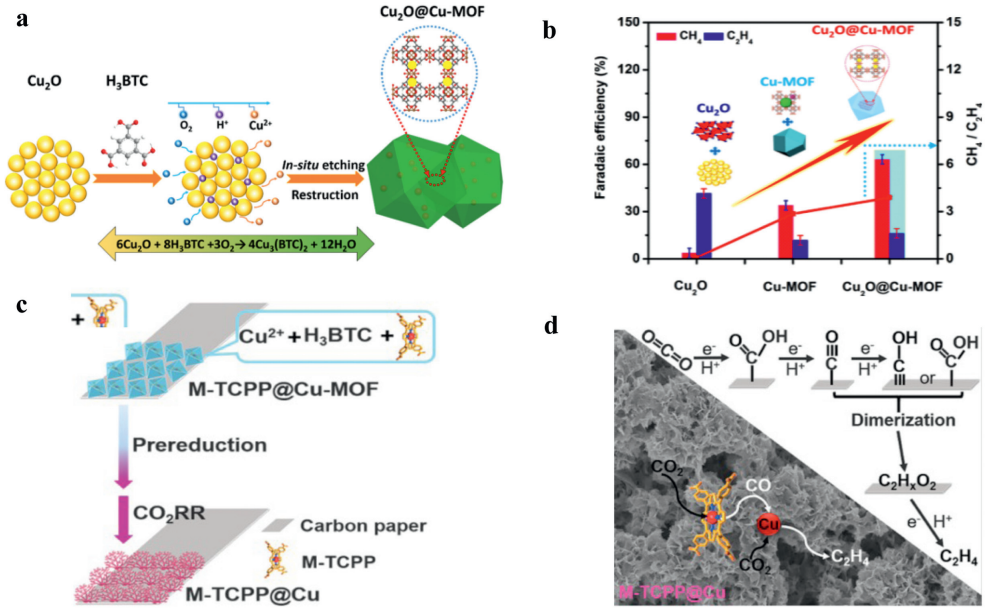

Fig. 5. Cu-based MOF as active supports. (a) Schematic illustration of the process to synthesize Cu_2O@Cu-MOF. Reproduced with permission [81]. Copyright 2019, American Chemical Society. (b) FEs of CH_4 and C_2H_4 and the ratio of CH_4 to C_2H_4 for Cu_2O@Cu-MOF, Cu-MOF, and Cu_2O at −1.71 V *vs.* RHE in CO_2-saturated 0.10 mol/L $KHCO_3$ solution. Reproduced with permission [81]. Copyright 2019, American Chemical Society. (c) Schematic illustration of preparation and CO_2ER of M-TCPP@Cu electrode. Reproduced with permission [82]. Copyright 2021, American Chemical Society. (d) Possible reaction route of the CO_2ER to C_2H_4. Reproduced with permission [82]. Copyright 2021, American Chemical Society.

and metal (FeCl, Co, and Ni) 5,10,15,20-tetraphenylporphyrin (M-TPPs) [82].

Sun *et al.* prepared a novel catalyst using CuO NPs anchored on Cu-MOF nanosheets *via* a facile solvothermal method. The catalyst delivered excellent performances with a FE of 50.00% for C_2H_4 at −1.10 V *vs.* RHE and outstanding stability even after long-term experiment. The marvelous performances can be attributed to the interface between CuO and Cu-MOF which could adsorb and activate CO_2 molecules [83].

The atomic layer infiltration (ALI) technique was used to fabricate an HKUST-1–5C-Zn catalyst which used Cu-MOF as active support with highly dispersed Zn atoms. Attributed to the uniform distribution of Zn-O-Zn sites on HKUST-1 which contributed to the CO_2 adsorption and formation of COOH*, it exhibited excellent performance in production of CO with a FE of ~80.00% at −1.80 V [84].

3. Conclusions and outlook

As a promising technology, the CO_2ER is essential in solving the global climate and environmental problems caused by the increasing CO_2 emissions. As interesting electrochemical catalysts, Cu-based MOFs have been receiving widespread interest from scholars owing to their porous structures and properties, and recently, the research interest and number of studies have been increasing.

In this minireview, we summarized the recent works on Cu-based MOFs and their derivatives as electrocatalysts for the CO_2ER. Cu-MOF catalysts offer several advantages for the CO_2ER process, which are attributed to their facile synthetic route, porous structure, and multiple active sites. When Cu-MOFs are directly used as catalysts, the discrete Cu atoms can provide active sites, and organic linkers can be modified to form active sites or charge-transfer agents. Further, their porous structure, formed by metal particles and the organic phase, facilitates the reaction with CO_2 or their application as catalyst supports. In addition, carbon-based catalysts with more highly dispersed metal particles can be obtained, using Cu-MOFs or their derivatives as precursors. The metal active sites inherited from Cu-MOFs maintain their catalytic activity and conductivity, facilitating the realization of efficient single-point catalysis. The MOF structure, which is tunable, can be employed to further construct bimetallic or even polymetallic structures, which would enable the facile synthesis of metal alloys and the design of efficient catalysts for the CO_2ER.

However, Cu-MOFs catalysts, similar to traditional MOF catalysts, still suffer from poor chemical stability. Thus, further improvement is required, as it is still difficult to conduct detection and analysis processes after the reaction. The Cu-MOF catalysts obtained by pyrolysis and the electrochemical method have significantly stable structures and exhibit excellent catalytic activities. Future studies are suggested to address these properties in literatures. In addition, new methods and strategies are recommended to fabricate Cu-MOF with more stable structures and excellent chemical activity. For instance, incorporated with highly conductive and active materials (graphene, carbon-based catalysts, *etc.*) will help enhance the electrochemical activity and stability. Besides, due to the complexity and diversities of the Cu-MOF based structures, machine learning can be applied to design efficient Cu-MOF and its derivatives as electrocatalysts for CO_2ER. These properties and recommendations highlight their significant un-

tapped potential for future application in environmental remediation.

Declaration of competing interest

The authors declare no competing financial interest.

Acknowledgments

This work was financially supported by the National Natural Science Foundation of China (Nos. 22003041 and 51902204) and Shenzhen Innovative Research Team Program (No. KQTD20190929173914967).

References

[1] C. Costentin, M. Robert, J.M. Savéant, Chem. Soc. Rev. 42 (2013) 2423–2436.
[2] J. Qiao, Y. Liu, F. Hong, J. Zhang, Chem. Soc. Rev. 45 (2014) 631–675.
[3] H.R.M. Jhong, S. Ma, P.J. Kenis, Curr. Opin. Chem. Eng. 2 (2013) 191–199.
[4] Y. Hori, Electrochemical CO_2 Reduction on Metal Electrodes, Springer, New York, 2008.
[5] H. Dau, C. Limberg, T. Reier, et al., ChemCatChem 2 (2010) 724–761.
[6] S.S. Chadwick, Ref. Serv. Rev. 16 (1988) 31–34.
[7] K.P. Kuhl, E.R. Cave, D.N. Abram, T.F. Jaramillo, Energy Environ. Sci. 5 (2012) 7050–7059.
[8] C. Oloman, H. Li, ChemSusChem 1 (2008) 385–391.
[9] S. Nitopi, E. Bertheussen, S.B. Scott, X. Liu, I. Chorkendorff, Chem. Rev. 119 (2019).
[10] M.B. Gawande, A. Goswami, F.O.X. Felpin, et al., Chem. Rev. 116 (2016) 3722.
[11] Y. Zhou, X.J. Guo, X.J. Li, et al., J. CO_2 Util. 37 (2020) 188–194.
[12] H. Lv, F. Lv, H. Qin, X. Min, B. Liu, CCS Chem. 3 (2021) 1435–1444.
[13] Y. Hori, A. Murata, R. Takahashi, J. Chem. Soc. Faraday Trans. 85 (1989) 2309–2326.
[14] K.P. Kuhl, T. Hatsukade, E.R. Cave, et al., J. Am. Chem. Soc. 136 (2014) 14107–14113.
[15] A.A. Peterson, F. Abild-Pedersen, F. Studt, J.R. Osmiumsl, J.K. Nerskov, Energy Environ. Sci. 3 (2010) 1311–1315.
[16] J.M. Spurgeon, B. Kumar, Energy Environ. Sci. 11 (2018) 1536–1551.
[17] C.W. Li, J. Ciston, M.W. Kanan, Nature 508 (2014) 504–507.
[18] I. Takahashi, O. Koga, N. Hoshi, Y. Hori, J. Electroanal. Chem. 533 (2002) 135–143.
[19] Y. Hori, I. Takahashi, O. Koga, N. Hoshi, J. Phys. Chem. B 106 (2002) 15–17.
[20] C. Hahn, T. Hatsukade, Y.G. Kim, A. Vailionis, T.F. Jaramillo, Proc. Natl. Acad. Sci. 114 (2017) 5918–5923.
[21] Y. Hori, I. Takahashi, O. Koga, N. Hoshi, J. Mol. Catal. A: Chem. 199 (2003) 39–47.
[22] E. Bertheussen, T.V. Hogg, Y. Abghoui, et al., ACS Energy Lett. 3 (2018) 634–640.
[23] A. Bagger, W. Ju, A.S. Varela, P. Strasser, J. Rossmeisl, ChemPhysChem 18 (2017) 3266–3273.
[24] H. Ooka, M.C. Figueiredo, M.T.M. Koper, Langmuir 33 (2017) 9307–9313.
[25] Y. Hori, A. Murata, Y. Yoshinami, J. Chem. Soc. Faraday Trans. 87 (1991) 125–128.
[26] P. Shao, L. Yi, S. Chen, T. Zhou, J. Zhang, J. Energy Chem. 29 (2020) 156–170.
[27] A.S. Varela, W. Ju, P. Strasser, Adv. Energy Mater. 8 (2018) 1703614–1703635.
[28] X. Liu, T. Yue, K. Qi, et al., Chin. Chem. Lett. 9 (2019) 2189–2201.
[29] D.D. Ma, S.G. Han, C. Cao, et al., Energy Environ. Sci. 14 (2021) 1544–1552.
[30] M.K. Hu, S. Zhou, D.D. Ma, Q.L. Zhu, Appl. Catal. B: Environ. 310 (2022) 121324.
[31] C. Cao, Q. Xu, Q.L. Zhu, Chem. Catal. 2 (2022) 693–723.
[32] B. Zhang, J. Zhang, J. Energy Chem. 26 (2017) 1050–1066.
[33] J. Albo, M. Perfecto-Irigaray, G. Beobide, A. Irabien, J. CO_2 Util. 33 (2019) 157–165.
[34] J. Hu, Y. Liu, J. Liu, C. Gu, AIChE J. 66 (2020) 16835.
[35] C.L. Rooney, Y. Wu, D.J. Gallagher, H. Wang, Nat. Sci. 1 (2022) 1–8.
[36] K. Kim, P. Wagner, K. Wagner, A.J. Mozer, Fuel 36 (2022) 4653–4676.
[37] R. Angamuthu, P. Byers, M. Lutz, A.L. Spek, E. Bouwman, Science 327 (2010) 313–315.
[38] R. Hinogami, S. Yotsuhashi, M. Deguchi, ECS Electrochem. Lett. 1 (2012) H17–H19.
[39] R.S. Kumar, S.S. Kumar, M.A. Kulandainathan, Electrochem. Commun. 25 (2012) 70–73.
[40] T. Maihom, S. Wannakao, B. Boekfa, J. Limtrakul, J. Phyc. Chem. C 117 (2013) 17650–17658.
[41] J. Albo, D. Vallejo, G. Beobide, ChemSusChem 10 (2017) 1100–1109.
[42] B. Rungtaweevoranit, J. Baek, J.R. Araujo, Nano Lett. 16 (2016) 7645–7649.
[43] C.W. Kung, C.O. Audu, A.W. Peters, ACS Energy Lett. 2 (2017) 2394–2401.
[44] Y.L. Qiu, H.X. Zhong, T.T. Zhang, ACS Appl. Mater. Interfaces 10 (2018) 2480–2489.
[45] B. An, Z. Li, Y. Song, Nat. Catal. 2 (2019) 709–717.
[46] Z. Weng, Y.S. Wu, M.Y. Wang, Nat. Commun. 9 (2018) 415.
[47] F. Yang, A.L. Chen, P.L. Deng, Chem. Sci. 10 (2019) 7975–7981.
[48] J.X. Wu, S.Z. Hou, X.D. Zhang, Chem. Sci. 10 (2019) 2199–2205.
[49] Z. Meng, J. Luo, W. Li, K.A. Mirica, J. Am. Chem. Soc. 142 (2020) 21656–21669.
[50] L. Majidi, A. Ahmadiparidari, N.N. Shan, Adv. Mater. 33 (2021) 2004393–2004401.
[51] S.M. Hwang, S.Y. Choi, M.H. Youn, ACS Omega 5 (2020) 23919–23930.
[52] Y. Han, S. Zhu, S. Xu, ChemElectroChem 8 (2021) 3174–3180.
[53] A. Ahmad, N. Iqbal, T. Noor, J. CO_2 Util. 48 (2021) 101523.
[54] H. Sun, L. Chen, L.K. Xiong, Nat. Commun. 12 (2021) 6823–6834.
[55] Y.H. Xiao, Y.X. Zhang, R. Zhai, Z.G. Gu, J. Zhang, Sci. China Mater. 1 (2021) 1–7.
[56] K. Zhao, Y.-M. Liu, X. Quan, S. Chen, H.T. Yu, ACS Appl. Mater. Interfaces 9 (2017) 5302–5311.
[57] D. Nam, O.S. Bushuyev, J. Li, J. Am. Chem. Soc. 140 (2018) 11378–11386.
[58] Y. Hou, Y.B. Huang, Y.L. Liang, G.L. Chai, R. Cao, CCS Chem. 1 (2019) 384–395.
[59] J. Liu, L. Peng, Y. Zhou, ACS Sustain. Chem. Eng. 7 (2019) 15739–15746.
[60] W. Guo, X. Sun, C. Chen, Green Chem. 21 (2019) 503–508.
[61] Y.S. Cheng, X.P. Chu, M. Ling, Catal. Sci. Technol. 9 (2019) 5668–5675.
[62] H. Zhong, M. Ghorbani-Asl, K.H. Ly, J. Zhang, X. Feng, Nat. Commun. 11 (2020) 1409–1419.
[63] K. Yao, Y. Xia, J. Li, J. Mater. Chem. A 8 (2020) 11117–11123.
[64] A.X. Guan, Z. Chen, Y.L. Quan, ACS Energy Lett. 5 (2020) 1044–1053.
[65] S.M. Cao, H.B. Chen, B.X. Dong, J. Energy Chem. 54 (2021) 555–563.
[66] S.M. Cao, H.B. Chen, M.J. Liu, J. CO_2 Util. 44 (2021) 101418.
[67] Y.Y. Zhang, K. Li, M.M. Chen, ACS Appl. Nano Mater. 3 (2020) 257–263.
[68] N. Sikdar, J.R.C. Junqueira, S. Dieckhofer, Angew. Chem. Int. Ed. 60 (2021) 23427–23434.
[69] S.M. Li, Y. Shi, J.J. Zhang, ChemSusChem 14 (2021) 2050–2055.
[70] X. Ma, J. Tian, M. Wang, Catal. Sci. Technol. 11 (2021) 6096–6102.
[71] S. Juntrapirom, J. Santatiwongchai, A. Watwiangkham, Catal. Sci. Technol. 11 (2021) 8065–8078.
[72] H.D. Jin, L.K. Xiong, X. Zhang, Acta Phys. Chim. Sin. 37 (2021) 2006017.
[73] X. Yang, J. Cheng, X. Yang, Chem. Eng. J. 431 (2022) 134171.
[74] Y. Xue, C. Li, X. Zhou, ChemElectroChem 9 (2022) e202101648.
[75] N. Sikdar, J.R.C. Junqueira, D. Öhl, Chem. Eur. J. 28 (2022) e202104249.
[76] M.K. Kim, H.J. Kim, H. Lim, Y. Kwon, H.M. Jeong, Electrochim. Acta 306 (2019) 28–34.
[77] Q.G. Zhu, D.X. Yang, H.Z. Liu, Angew. Chem. Int. Ed. 59 (2020) 8896–8901.
[78] W.Y. Zhi, Y.T. Liu, S.L. Shan, J. CO_2 Util. 50 (2021) 101594.
[79] H. Zhang, Y. Yang, Y.X. Liang, ChemSusChem 14 (2021) 1–8.
[80] D. Wang, J.L. Xu, Y. Zhu, Chemosphere 278 (2021) 130408.
[81] X.Y. Tan, C. Yu, C.T. Zhao, ACS Appl. Mater. Interfaces 11 (2019) 9904–9910.
[82] T. Yan, J.H. Guo, Z.Q. Liu, W.Y. Sun, ACS Appl. Mater. Interfaces 13 (2021) 25937–25945.
[83] L. Wang, X. Li, L. Hao, Chin. J. Catal. 43 (2022) 1049–1057.
[84] X. Han, Z. Liu, M. Cao, Chem. Mater. 1 (2022) 1–8.